IEEE Access
Multidisciplinary | Rapid Review | Open Access Journal

Received 12 January 2024, accepted 12 February 2024, date of publication 14 February 2024, date of current version 22 February 2024.

Digital Object Identifier 10.1109/ACCESS.2024.3366452

RESEARCH ARTICLE

Higher Order Bandpass Single and Dual Band Frequency Selective Surfaces With Aperture Coupled Patch Resonators

K. N. MOHAN, (Student Member, IEEE), AND YOGESH KUMAR CHOUKIKER, (Senior Member, IEEE)

Department of Communication Engineering, School of Electronics Engineering (SENSE), Vellore Institute of Technology, Vellore, Tamil Nadu 632014, India

Corresponding author: Yogesh Kumar Choukiker (yogesh.ku.84@gmail.com)

This work was supported by Vellore Institute of Technology, Vellore, Tamil Nadu, India.

ABSTRACT In this article, a low profile aperture coupled single and dual band higher order bandpass frequency selective surface (FSS) is proposed. Initially, a basic patch resonator with L-shape truncated corner is investigated theoretically so that two orthogonal modes can be excited simultaneously. Next, to avoid the cross-polarized reflection produced by two orthogonal modes, a combination of four such L-shape truncated patch resonators with 90° between two adjoining patches are implemented and analyzed.Further, by arranging two of such combination resonators placed back-to-back manner through aperture coupling metallic layer in middle, a three layer single mode fourth order and a dual band second order bandpass FSS is designed. The proposed bandpass FSS enables higher order bandpass FSSs where the order of the modes is twice than traditional aperture coupled patch resonators (AC-PRs). It provides more flexibility at higher order filtering responses. To endorse the design concept, a single and dual bandpass FSS is simulated to initiate magnetic and electric coupling through the aperture metallic layer. Moreover, an equivalent circuit model for the even and odd mode analysis method is examined the principle of operation. Finally, the proposed bandpass FSS is fabricated and tested in a vector network analyzer (VNA) setup. The measured and simulated results are compared and validated.

INDEX TERMS AC-PRs, aperture coupled, dual mode, higher order FSS, patch resonators, polarization, single mode.

I. INTRODUCTION

Frequency selective surface (FSS) is an infinite array of elements periodically arranged as identical aperture elements or metallic patches. In electromagnetic (EM), FSS are exhibits filtering wave in space [1], [2]. They are designed to manipulate the amplitude, phase and polarization of incident waves. Among them, bandpass FSS allows one or several frequency waves through the structure and reject others [3], [4]. A traditional single layer topology bandpass FSS explored first order filtering, and failure to meet higher order single band in wireless communication systems [5], [6].

In order to develop higher order bandpass FSS, the single layer can be cascaded with quarter wavelength spacing. However, the overall size of thickness is very large and too bulky [7], [8]. In [9], bandpass FSS frequently used in multilayer topology at higher order frequency bands proposed with low profile, size reduction and less insertion loss. Followed by, a non-resonant element has been proposed in multilayer to obtain single-band higher order filtering [10]. Still, the order of filtering is directly depends on number of layers and 2-dimensional (2-D) structure. Another approach to achieve higher order bandpass is 3-dimensional (3-D) cavity elements. It proposes superior features like more freedom of design [11], [12], [13]. However, these 3-D FSS are complicated in design and have large assembly tolerances.

The associate editor coordinating the review of this manuscript and approving it for publication was Chinmoy Saha.

Another remarkable approach to multilayer topology is aperture coupled patch resonators (AC-PRs). The aperture layer is proposed in the middle of top and bottom metallic layers to achieve flexible higher order filtering FSS [14]. Based on proposed structure, AC-PRs different concepts are developed to obtain single and dual-order bandpass FSS [15], [16], [17], [18], [19], [20]. In [15] non-resonant coupling apertures are placed at the position of where magnetic field intensities are high in the patch resonators, it is providing magnetic coupling between metallic patch layers in back to back manner based on filter theory [21]. In [16], FSS on dominant electric coupling AC-PRs proposed. Here, near the skirts of passband where two transmission zeros are presented to enhance frequency selectivity. In [17], to improve the frequency selectivity and higher order filtering based on AC-PRs with resonant aperture coupling proposed, called antenna-filter-antenna (AFA) model. The proposed model has notable advantages of higher order frequency selectivity with low profile, stable filtering absorption or reflection under different incident wave angles.The above mentioned works are proposed with cross polarized absorption or reflection by AC-PRs FSS.

In this article, an aperture coupled single mode and dual mode patch resonator bandpass FSS is proposed to realize higher-order filtering, where resonant modes are enlarged than classic AC-PRs. First, to generate two orthogonal modes by patch at two different frequencies, an L-shape truncated corner square patch is designed. Then, four L-shape corner-truncated patch resonators are placed with 90° rotations to eliminate cross-polarized reflection produced by two orthogonal modes. Further, combined L-shape truncated patches are positioned back-to-back through an aperture coupling metallic layer on middle. As per expectations, the middle metallic aperture layer obtained electric and magnetic couplings. In results, we obtained single and dual band higher order bandpass by proposed structure. To examine the principle of operation by proposed bandpass FSS, the equivalent circuit model is designed and analyzed. The proposed work is organized as follows: The operation principle of single and four square patches with L-shape truncation is examined in section II. In section III, single-band fourth-order bandpass FSS is designed and the respective equivalent circuit model is analyzed. In section IV, dual band second order bandpass is designed and equivalent circuit model is analyzed. Finally, a fabricated prototype of proposed bandpass FSS is measured to verify the concept in section V.

II. SINGLE BAND DUAL MODE PATCH RESONATOR

To achieve the circular polarization and band-pass filter in the patch, truncation corner is the well known technique [21], [22], [23], [24]. It is used to control the resonant properties of the dual mode patch resonator along diagonal lines. This approach is expanded to create dual-mode FSS resonators.

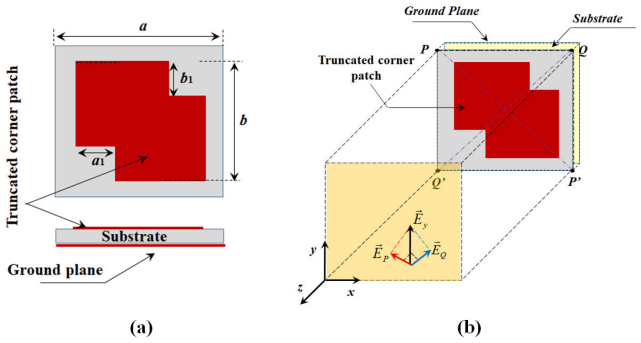

FIGURE 1. Proposed L-shape truncated patch resonator (a) Geometry of patch resonator (b) simulation setup (Dimensions:: a=8mm, b=5.3mm, a_1=b_1=1.3mm).

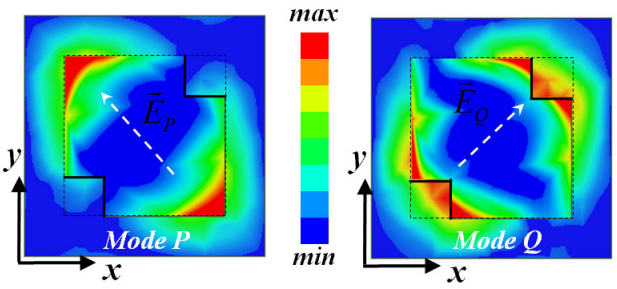

FIGURE 2. Surface current distribution of patch resonator for different modes (Mode P and Mode Q).

A. ANALYSIS OF SINGLE PATCH RESONATOR

The geometry of the diagonal corner L-shape truncated single patch resonator is shown in Fig. 1(a). The proposed resonator has two layers, top layer (L-shape truncated patch) and bottom layer (metallic conductor). It provides a dual mode along the diagonal lines. It is printed on top of the Rogers 4003 (ε_r=3.55) substrate with height h=0.813mm and backed by metallic ground plane. The proposed patch resonator is placed inside the waveguide in simulation as shown in Fig. 1(b). The incidence of a linearly polarized EM wave and periodic boundary conditions (PBCs) are applied along x- and y-axis. Under cavity modes operation, the field intensities are concentrated between the top and bottom layer of the patch resonator due to completely covered with ground plane. Therefore, the incident wave is completely reflected and only reflection coefficients may be obtained.

To show the working mechanism of the proposed patch resonator, the electric field vector is divided into two orthogonal modes and equal components $\vec{E}_P^i$ and $\vec{E}_Q^i$ along the lines PP' and QQ' as shown in Fig. 1(b). These two orthogonal modes are represents as mode P and mode Q, and have different resonant frequencies due to the L-shape truncation of diagonal corners. Therefore, based on structure symmetry, x or y-polarized incident electirc-field component can only excites mode P or mode Q as shown in Fig. 2. Hence, it generates reflected component either $\vec{E}_P^r$ or $\vec{E}_Q^r$.

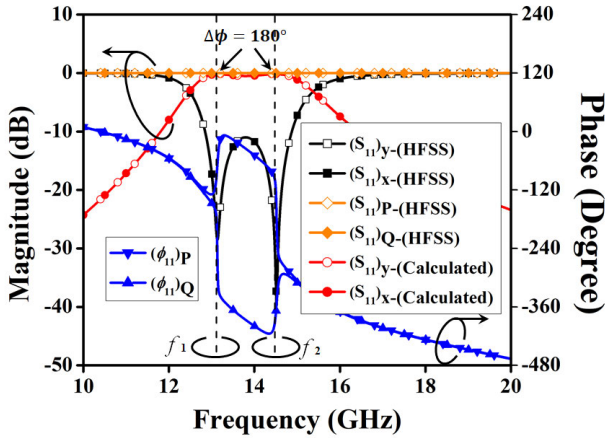

FIGURE 3. Magnitude of S-parameter and phase of the proposed patch resonator under *y*-polarized incidence for both modes.

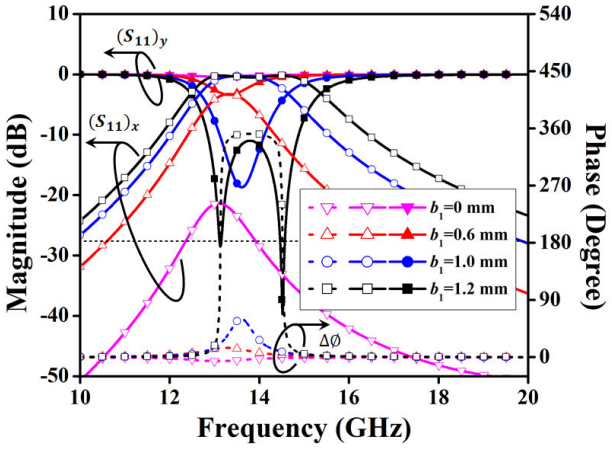

FIGURE 4. Parametric study (S-parameter magnitude and phase) of the proposed patch resonator for different b_1 values under *y*-polarised incidence.

The reflected $\overrightarrow{E_P^r}$ or $\overrightarrow{E_Q^r}$ can be stated using coordinate transformations as

$$\overrightarrow{E_P^r} = \frac{1}{2}(\overrightarrow{e_y} - \overrightarrow{e_x}) \mid \overrightarrow{E_y^r} \mid (S_{11})_P \tag{1}$$

$$\overrightarrow{E_Q^r} = \frac{1}{2}(\overrightarrow{e_y} + \overrightarrow{e_x}) \mid \overrightarrow{E_y^r} \mid (S_{11})_Q \tag{2}$$

where $(S_{11})_P = \mid S_{11} \mid_P e^{j(\phi_{11})_P}$ and $(S_{11})_Q = \mid S_{11} \mid_Q e^{j(\phi_{11})_Q}$ are reflected coefficients of total resonator in-terms of $\overrightarrow{E_P^i}$ and $\overrightarrow{E_Q^i}$. Thus, the total reflected electric-field vector $\overrightarrow{E^r}$ may be computed as

$$\begin{aligned}\overrightarrow{E^r} &= \overrightarrow{E_P^r} + E_Q^r \\ &= \frac{1}{2}(\overrightarrow{e_y} - \overrightarrow{e_x}) \mid \overrightarrow{E_y^r} \mid (S_{11})_P + \frac{1}{2}(\overrightarrow{e_y} + \overrightarrow{e_x}) \mid \overrightarrow{E_y^r} \mid (S_{11})_Q \end{aligned} \tag{3}$$

$$= \overrightarrow{e_y} \mid \overrightarrow{E_y^r} \mid (S_{11})_x + \overrightarrow{e_x} \mid \overrightarrow{E_x^r} \mid (S_{11})_y = \overrightarrow{E_y^r} + \overrightarrow{E_x^r} \tag{4}$$

where, $(S_{11})_y$ and $(S_{11})_x$ are the x-polarised (cross-polarized) and y-polarised (co-polarized) reflection coefficient of the proposed patch resonator when y-polarised is incidence. It is written as
$(S_{11})_y = \frac{1}{2}((S_{11})_Q + (S_{11})_P) = \frac{1}{2}(|S_{11}|_Q e^{j(\phi_{11})_Q} + |S_{11}|_P e^{j(\phi_{11})_P}$ and
$(S_{11})_x = \frac{1}{2}((S_{11})_Q - (S_{11})_P) = \frac{1}{2}(|S_{11}|_Q e^{j(\phi_{11})_Q} - |S_{11}|_P e^{j(\phi_{11})_P}$

To obtain the $(S_{11})_P$ and $(S_{11})_Q$, the patch resonator should be under incidences of $\overrightarrow{E_P^i}$- and $\overrightarrow{E_Q^i}$-polarized EM waves. It is analyzed by using the full-wave simulator HFSS, as illustrated in Fig. 2. As can be seen, the proposed patch resonator have the polarised wave for both the modes (mode P and mode Q) under y-polarised incidence, respectively. Thereafter, the magnitude of S-parameter and phases of the proposed resonator is obtained for both the modes as shown in Fig. 3. It is noticed that for mode P and mode Q, the magnitude of S-parameter $|(S_{11})|_P$ and $|(S_{11})|_Q$ is unity which is around 0dB, whereas the phase responses $(\phi_{11})_P$ and $(\phi_{11})_Q$ are different. This is because of different resonant length of mode P and mode Q. As a result, $(S_{11})_y$ and $(S_{11})_x$ can be obtained as:

$$S_{11} = \frac{1}{2}e^{j(\phi_{11})_P}(1 + e^{j\Delta\phi}) \tag{5}$$

$$S_{11} = \frac{1}{2}e^{j(\phi_{11})_Q}(1 - e^{j\Delta\phi}), \tag{6}$$

where $(\phi_{11})_P$ and $(\phi_{11})_Q$ are the phase of the patch resonator for mode P and mode Q, respectively. $\Delta\phi$ is the phase difference of the reflection coefficient between $(\phi_{11})_P$ and $(\phi_{11})_Q$. The phase difference occures only under incidences of $\overrightarrow{E_P^i}$- and $\overrightarrow{E_Q^i}$-polarized EM waves. As a result, there is co- and cross-polarized reflections. The magnitude of x- and y-polarized S-parameter is calculated from (5)-(6). It is well matched with simulated (HFSS) magnitude of x- and y-polarized S-parameter in entire band, as shown in Fig. 3. In addition, for cross-polarized reflection, a flat reflection band is formed, whereas, for co-polarized reflection, two reflection zeros at f_1 and f_2 are obtained at locations of $(\Delta\phi)$=180° in case of $(\Delta\phi)$=180°, $|(S_{11})_y| = 0$ and $|(S_{11})_y| = 1$, as seen in (5)-(6). Thereafter, y-polarized incident wave is then transformed entirely to x-polarized reflection, resulting in co-polarized reflection zeros. This process is comparable to that utilised in reflect arrays to twist the linearly polarised incident wave by 90° [21].

Next, Fig. 4 shows the parametric analysis of the proposed L-shape corner truncated patch resonator for cross- and co-polarized reflections and phase difference $(\Delta\phi)$. It is observed that, when $b_1 = 0mm$ (without corner truncation), the patch resonator works as a single-mode resonator under y-polarized incidence. Hence, the magnitude of S-parameter is $|(S_{11})_y| = 1$ and $|(S_{11})_x|$=0, and the phase difference $(\Delta\phi) = 0$ are obtained. As a result, co-polarized is occurs. Similarly, when b_1 increases, the y-polarized incidence wave is gradually converted to x-polarized reflection and the phase difference $\Delta\phi$ increases, as shown in Fig. 4. In case of

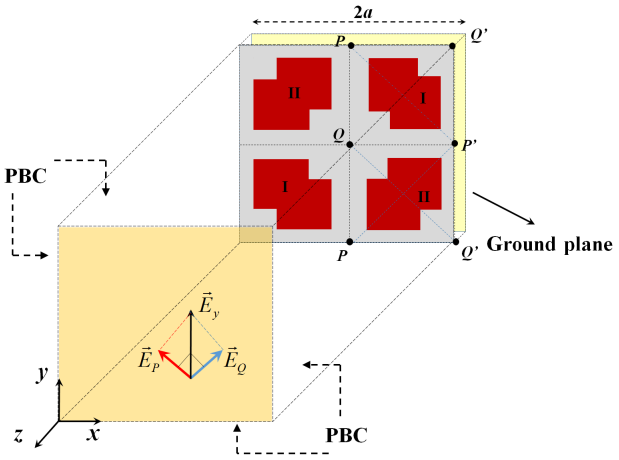

FIGURE 5. Geometry of combined four L-shape truncated patches and simulation set-up.

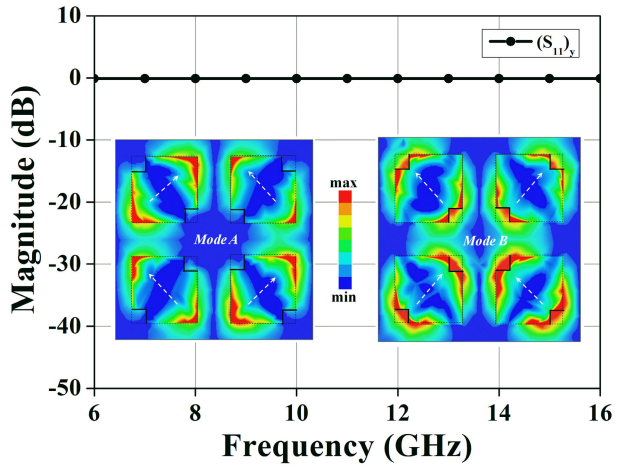

FIGURE 6. S-parameter magnitude (S_{11}) and surface current distribution for both mode under *y*-polarized incidence.

$b_1 = 1.2\ mm$, two particular frequencies fulfill the criteria of $(\Delta\phi) = 180°$ resulting in two co-polarized reflection zeros (or cross-polarized reflection poles), as seen in Fig. 3. Thus, it relies purely on the degree of corner truncation. As a result, the number of co-polarized (or cross-polarized) reflection zeros (or poles) is completely determined by the degree of L-shape corner truncation. It is concluded that the L-shape corner truncations may be used to convert a patch resonator from a single-mode resonator to a dual-mode resonator, providing extra resonances without increasing the number or size of the resonator.

B. ANALYSIS OF L-SHAPE CORNER TRUNCATED FOUR PATCH RESONATOR

A single-patch resonator with an L-shaped corner truncated produces a large amount of cross-polarized reflection due to the excitation of two orthogonal modes (mode P and mode Q). To overcome this issue, four L-shape corner-truncated patch resonators are placed with 90° rotation, as illustrated in Fig. 5. The surface current distribution of four patch resonators under *y*-polarized incidence is shown in Fig. 6. It is noticed that both modes (P and Q) are generated in each L-shape corner truncated patch resonator and dual-mode characteristics are maintained like single-patch resonator. In terms of the $x = a$ plane and the diagonal lines PP' and QQ', the proposed four patch resonator is symmetrical. Only the identical components along the *y*-axis may be found in the reflected $\overrightarrow{E_Q^r}$ and $\overrightarrow{E_Q^r}$, resulting in $(S_{11})_P = (S_{11})_Q$. Therefore, the total E-field vector $\overrightarrow{E^r} = \overrightarrow{E_y^r}$ and cross polarized reflection is zero $((S_{11})x = 0)$ as mentioned in (3). Thereafter, the magnitude of the co-polarized reflection coefficients is calculated as

$$|(S_{11})_y| = \frac{1}{2}|1 + e^{j(\Delta\phi)}| = 1 \tag{7}$$

where, the phase difference $\Delta\phi = (\Delta\phi_{11})_P - (\Delta\phi_{11})_Q$ is zero as shown in Fig. 6. Here, the magnitude of S-parameter under *y*-polarized incidence is 0dB. It is concluded that the proposed patch resonator is useful to design the frequency selective surface (FSS) element. Next section, describes the higher-order bandpass frequency selective surface using the proposed design.

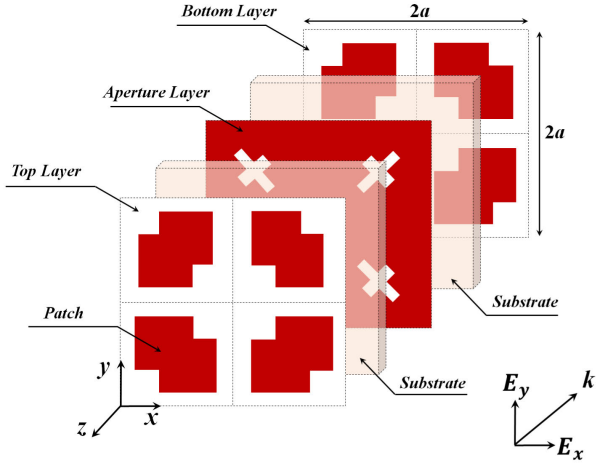

FIGURE 7. 3D geometry of proposed single band fourth order bandpass FSS.

III. APERTURE COUPLED SINGLE BAND FOURTH ORDER BANDPASS FSS

To create a bandpass FSS, the previously designed four element patch resonator shown in Fig. 5 was used. Two identical patch resonators are arranged in a back-to-back stacked configuration, as shown in Fig. 7. The proposed stacked configuration structure of the FSS element is made up of three metallic layers. The top and bottom layers consist of identical patch resonators, whereas the middle is a metallic layer etched with an aperture coupled structure (see Fig. 7). All three layers are separated by dielectric substrates. In addition, sub-element and cross section view of the proposed FSS shown in Fig. 8. The aperture slot

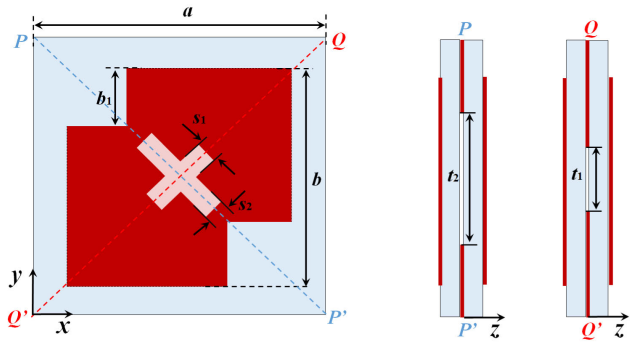

FIGURE 8. Sub-element and cross-section view of proposed single band fourth order bandpass FSS (Dimensions: $a = 8mm$, $b = 5.3mm$, b_1=1.2mm, $S_1 = S_2 = 1.1mm$, $t_1 = 1.8mm$, $t_2 = 2.7mm$).

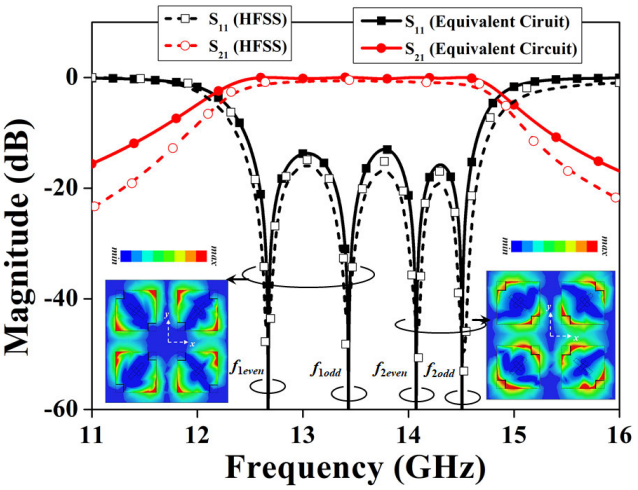

FIGURE 9. S-parameter magnitude and surface current distribution of the proposed single band fourth order bandpass FSS under *y*-polarized incidence.

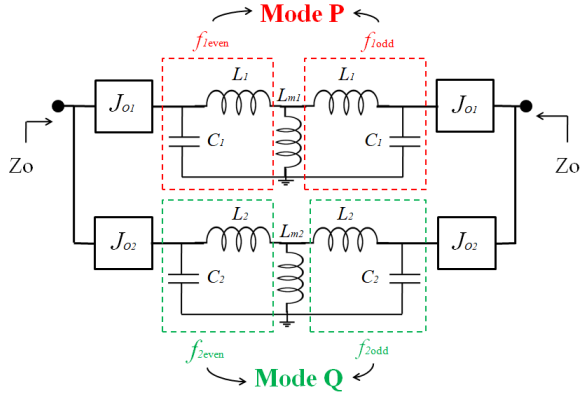

FIGURE 10. Equivalent circuit model of the proposed single band fourth order bandpass FSS (Circuit parameters: $L_1 = 0.184nH$, $C_1 = 0.8pF$, $L_2 = 0.096nH$, $C_1 = 1.27pF$, $L_{m1} = 0.07nH$, $L_{m2} = 0.004544nH$, J_{01}=0.0035714 S, J_{02}=0.0035714 S).

is etched in the middle layer, back side of the each patch resonator (top and bottom layer), and are also along the diagonal lines PP' and QQ'. The proposed geometry provides the four pole bandpass filtering response as shown in Fig. 9. The magnitude of S-parameters are obtained using HFSS simulation software under *y*-polarized incidence. It is noticed that between 12.2 GHz to 14.8 GHz four transmission poles ($f_{1even}, f_{1odd}, f_{2even}, f_{2odd}$) are obtained with passband bandwidth of 2.6 GHz and 21% fractional bandwidth (FBW).

Fig. 9 also shows the surface current distribution (E-field) of the proposed bandpass FSS for a clear understanding of the basic mechanism. It is observed that mode P generates f_{1even} and f_{1odd} transmission poles, whereas mode Q generates f_{2even} and f_{2odd} transmission poles. Furthermore, it is observed that at aperture coupling position the distribution of current is very less, it means the selection of aperture position is based on distribution of current (H-field). Hence, it conclude that the top and bottom FSS patch resonator are magnetically coupled by the cross-orthogonal apertures.

Next, the proposed FSS model is also explained with equivalent circuit model, as shown in Fig. 10. It is noticed that mode P and mode Q of the proposed FSS are represented by LC circuits, the resonant frequencies of which are defined by the dimensions of the dual mode patch resonator. The input and output ports are matched with characteristics impedance Z_o=120π, it is represents as a wave impedance in free space. Here, the inverter admittance J_{O1} and J_{O2} are utilised to indicate the coupling between input and output ports and also for both modes (modes P and Q). The inductance L_{m1}=$L_1 * k_{m1}$, L_{m2}=$L_2 * k_{m2}$ are defined as mutual inductance in aperture layer (middle layer) between top and bottom layer. Here, k_{m1} and k_{m2} are magnetic coupling coefficients in aperture layer. The even- and odd-mode analysis approach is then used to calculate these coupling coefficients. Moreover, even- and odd-mode analysis approach also used to calculate the resonant frequencies, $f_{1odd} = 1/(2\pi\sqrt{L_1C_1})$,$f_{1even} = 1/(2\pi\sqrt{(L_1 + 2L_{m1})C_1})$ and $f_{2odd} = 1/(2\pi\sqrt{L_2C_2})$, $f_{2even} = 1/(2\pi\sqrt{(L_2 + 2L_{m2})C_2})$, as shown in Fig. 10. Here, the odd-mode resonant frequencies are based on dual mode patch resonator whereas the even mode resonant frequencies are based on dual mode patch resonator and magnetic coupling in aperture layer. Hence, the magnetic coupling coefficient is calculated as $K_{m1} = x_1/(1 - x_1)$ and $K_{m2} = x_2/(1 - x_2)$, where $x_1 = \frac{(f_{1odd})^2-(f_{1even})^2}{(f_{1odd})^2+(f_{1even})^2}$ and $x_2 = \frac{(f_{2odd})^2-(f_{2even})^2}{(f_{2odd})^2+(f_{2even})^2}$. The coupling coefficients (K_{m1} and K_{m2}) are controlling the cross-orthogonal apertures because the E-field energy can only be coupled through the coupling aperture. Therefore, Fig. 11 shows the variation of coupling coefficient with dimensions of aperture. It is observed that coupling coefficients are individually expanded by increasing the sizes of apertures. Thereafter, all circuit parameters are calculated and using ADS circuit simulation software S-parameter curve is plotted, as shown in Fig. 9. It is noted that the 3D simulation (HFSS) and circuit simulation (ADS) results are well matched, and provide the single band fourth order bandpass characteristics. Moreover, based on the comparison, it was found that slight adjustments to the dimensions of FSSs

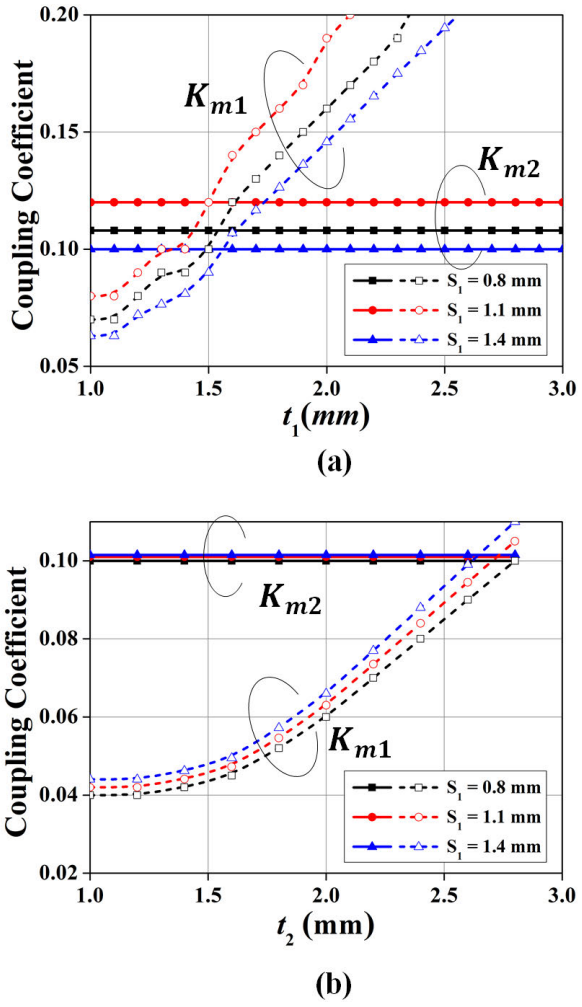

FIGURE 11. Parametric study of magnetic coupling coefficients (K_{ma} and $Km2$) for different aperture dimensions (S_1 and S_2).

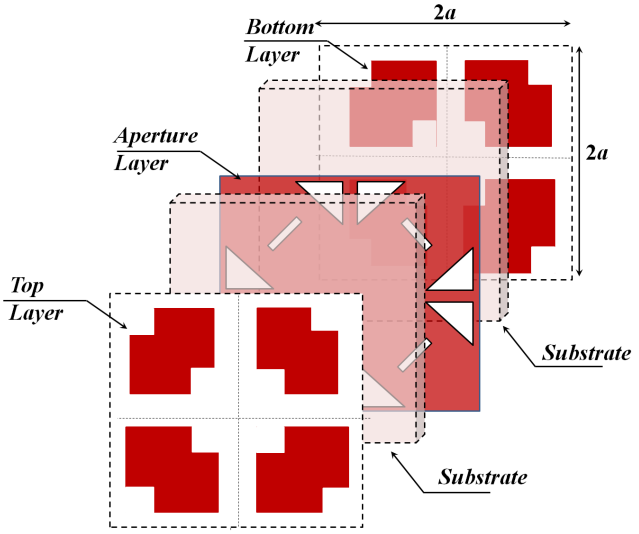

FIGURE 12. 3D geometry of proposed dual band second order bandpass FSS.

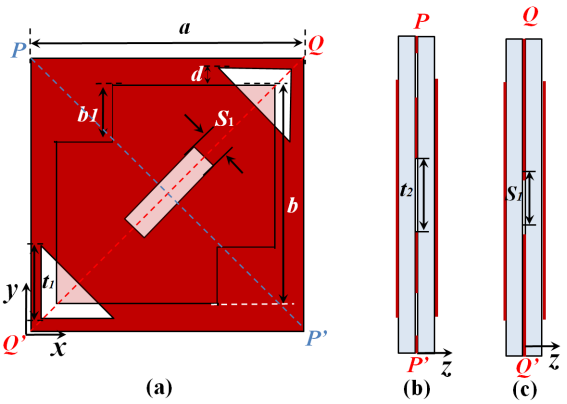

FIGURE 13. Sub-element and cross-section view of proposed dual band second order bandpass FSS (Dimensions: a=8mm, b=6.7mm, b_1=1.75mm, S_1=0.415mm, t2=1.3mm, d=0.4mm, h=0.406mm, ε_r = 3.55).

were required in order to ensure that all transmission poles were placed in the desired locations.

IV. APERTURE COUPLED DUAL BAND SECOND ORDER BANDPASS FSS

In section III, a single band fourth order aperture coupled has been proposed. With the proposed geometry, a dual band higher order bandpass FSS also can be realized, as shown in Fig. 7. The difference is that the trinangular apertures are replaced by one of the cross orthogonal apertures, which is placed near the un-truncated edges of the patches shown in Fig. 12. All three layers are separated by dielectric substrates. In addition, sub-element and cross section view of the proposed FSS shown in Fig. 13. The aperture slot is etched from the middle layer, back side of the each patch resonator (top and bottom layer), and are also along the diagonal lines PP' and QQ'. The proposed geometry provides the dual band second order bandpass filtering response as shown in Fig. 14. The magnitude of S-parameters are obtained using HFSS simulation software under *y*-polarized incidence. It is noticed that between 8.5 GHz to 11.5 GHz four transmission poles (f_{1even}, f_{1odd}, f_{2even}, f_{2odd}) are obtained with two passband around 8.5 GHz and 11.5 GHz with low band ratio of 1.27, and fractional bandwidth (FBW) of 6.1% at first passband, 4.2% at second passband. Moreover, the two transmission zeros located near to the passband between the two operation bands.

Fig. 15 shows the surface current distribution (E-field) of the proposed dual bandpass FSS for a clear understanding of the basic mechanism. It is observed that mode P generates f_{1even} and f_{1odd} of first passband, whereas mode Q generates f_{2even} and f_{2odd} of second passband consequently. Furthermore, it is observed that at aperture coupling position the distribution of current is very less, it means that selection of aperture position is based on distribution of current (E/H-field). Hence, it conclude that the top and bottom FSS patch resonator are electrically coupled by

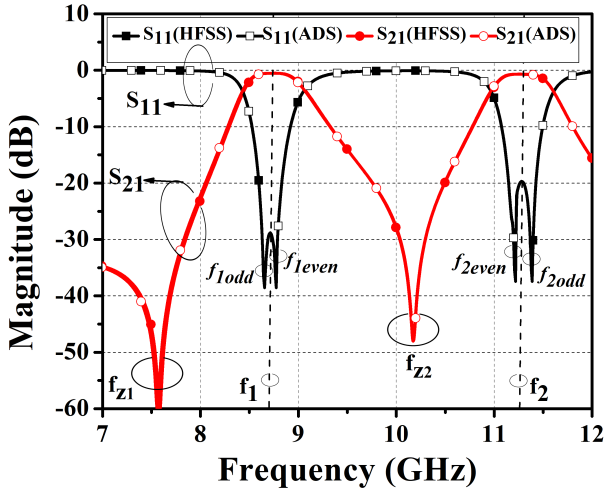

FIGURE 14. S-parameters under y-polarized incidence (HFSS) and equivalent circuit simulation (ADS).

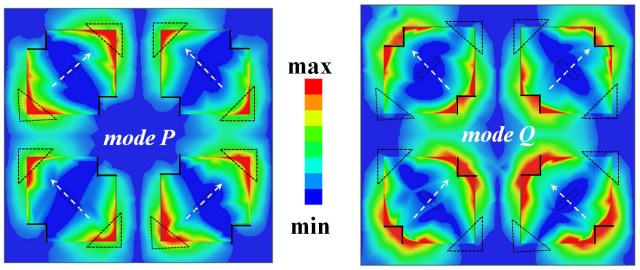

FIGURE 15. magnitude and surface current distribution of the proposed dual band second order bandpass FSS under *y*-polarized incidence, (a) mode P, (b) mode Q.

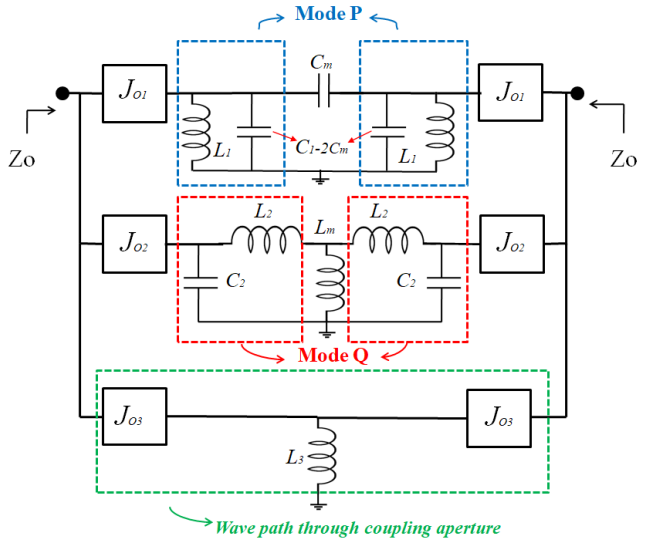

FIGURE 16. Equivalent circuit model of aperture coupled dual band FSSs, $L_1 = 0.225nH, C_1 = 1.5pF, C_m = 0.03pF, L_2 = 0.114nH, C_2 = 1.8pF, J_{O1} = 0.0019S, J_{O2} = 0.000311S, L_m = 0.0045nH, L_3 = 0.207nH, J_{O3} = 0.000209$.

triangular aperture at first passband, while the both rectangle and triangular aperture are magnetically coupled at second passband respectively. In addition, the transmission zeros near to the first passband at both sides are produced by coupling between the signal path through the triangular aperture [20].

Next, the proposed FSS are represented by LC circuits in Fig. 16., the resonant frequencies of which are defined by the dimensions of the dual mode patch resonator. The input and output ports are matched with characteristics impedance Z_o=120π, it is represents as a wave impedance in free space. Here, the inverter admittance J_{01}, J_{02} and J_{03} are utilised to indicate the coupling between input and output ports and also for both modes (modes P and Q). The electrically coupled represents by mutual capacitance C_m=$C_1 * K_e$. Similarly, the inductance L_m=$L_2 * k_m$ is defined as mutual inductance in aperture layer (middle layer) between top and bottom layer. The even- and odd-mode analysis approach is then used to calculate these coupling coefficients. Moreover, even- and odd-mode analysis approach also used to calculate the resonant frequencies, $f_{1odd} = 1/(2\pi\sqrt{L_1C_1})$,$f_{1even} = 1/(2\pi\sqrt{(L_1(C_1 - 2C_m)}$ and $f_{2odd} = 1/(2\pi\sqrt{L_2C_2})$, $f_{2even} = 1/(2\pi\sqrt{(L_2 + 2L_m)C_2})$, as shown in Fig. 16. Here, the odd-mode resonant frequencies are based on dual mode patch resonator whereas the even mode resonant frequencies are based on coupling in aperture. Hence, the coupling coefficient is calculated as $K_e = x_1/(1 - x_1)$ and $K_m = x_2/(1 - x_2)$, where $x_1 = \frac{(f_{1even})^2-(f_{1odd})^2}{(f_{1even})^2+(f_{1odd})^2}$ and $x_2 = \frac{(f_{2odd})^2-(f_{2even})^2}{(f_{2odd})^2+(f_{2even})^2}$. The coupling coefficients (K_e is electric coupling coefficients provided by triangular aperture, and K_m) is magentic coupling coeffiencients by rectangular aperture, which is familiar to Fig. 10. Thus, the E/H-field energy can only be coupled through the coupling aperture. Therefore, Fig. 17 shows the variation of coupling coefficient with dimensions of aperture. It is observed that coupling coefficients are individually expanded by increasing the sizes of apertures. Finally, all the circuit parameters are calculated and using ADS circuit simulation software S-parameter curve is plotted, as shown in Fig. 14. It is noted that the 3D simulation (HFSS) and circuit simulation (ADS) results are well matched, and provide the dual band second order bandpass characteristics. Moreover, based on the comparison, it was found that slight adjustments to the dimensions of FSSs were required in order to ensure that all transmission poles were placed in the desired locations. Next section describes the designed prototype and experimental verification of the proposed dual band second order bandpass FSS.

V. EXPERIMENTAL VALIDATION

In order to validate the simulation results, the prototype of the proposed bandpass FSS was fabricated and measured as shown in Fig. 18. The fabricated prototype of the top and bottom layer shown in Fig. 18(a). It is printed on RO4003C dielectric substrates (thickness=0.813 mm and 0.406mm) with dielectric constant $\varepsilon_r = 3.55$ and loss tangent tan(δ) = 0.0029. The size of the proposed FSS is 80 $\times$ 80mm^2 and

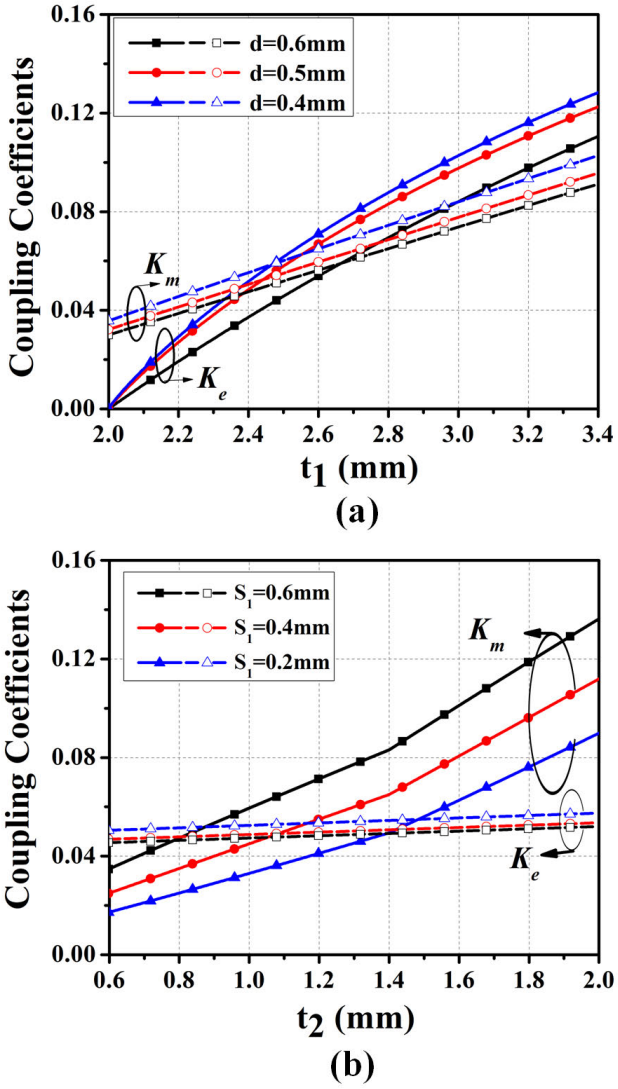

FIGURE 17. Parametric study of magnetic coupling coefficients (K_m and Ke) for different aperture dimensions (t_1 and t_2).

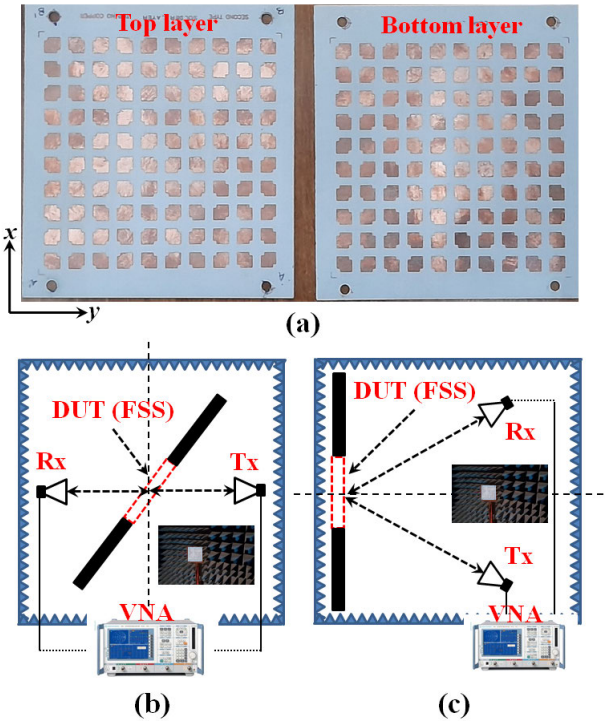

FIGURE 18. Proposed L-shape truncated dual band second order FSS (a) Fabricated prototype (b) transmission coefficient measurement setup (c) reflection coefficient measurement system.

has 10 × 10 elements for single band and 120 × 120mm^2 for dual band FSS. The fabricated prototype S-parameters were measured using vector network analyser (VNA) and filter characteristics under different angles were measured in anechoic chamber, both available at the Antenna Design LAB, VIT, Vellore, India. Fig. 12(b) and (c) shows the measurement set-up in anechoic chamber for transmission and reflection coefficient measurement and obtained results for the proposed FSS are discussed in this Section.

During the measurement of transmission and reflection coefficient parameters the fabricated prototype of bandpass FSS and Tx/Rx (Horn antenna) has been used. In case of transmission coefficient measurement, rotatable screen was placed in center between Tx/Rx (see Fig. 18(b)). The distance (D) between the device under test (DUT-FSS) and Tx/Rx should satisfy the far-field distance requirement of the antennas. While recording the data of the transmission coefficient, we have to properly rotate the (DUT-FSS) screen or the antennas to the desired angle θ. In case of reflection coefficient measurement, rotatable screen was placed on the wall of the anechoic chamber with fixed 0° angle between Tx/Rx (see Fig. 18(c)). The distance (D) between (DUT-FSS) and Tx/Rx should satisfy the far-field distance requirement of the antennas. While recording the data of the reflection coefficient, we have to properly rotate the Tx/Rx horn antenna in desired angle θ. To minimise the impacts of environmental noise, numerous reflections, and EM wave propagation loss, different cases were used, first FSS sized empty window, then copper plate placed between Tx/Rx antennas and finally fabricated prototype is mounted between the horn antennas. The complete measurement of the proposed FSS is based on a free space measurement system [23], [24], [25], [26]. The measured reflection and transmission coefficient of the proposed bandpass FSS is shown in Fig. 19(a) and Fig 20(a) for x-polarised incidence case and different θ angles from 0° to 60°. It is observed that S-parameter magnitude is stable for x-polarised and different angles. Moreover, the measured minimum and maximum insertion loss (S_{21}) for the single band FSS in range of is 1.1dB to 4.8dB and dual band range is 0.1dB to 3dB. Similarly, in case y-polarised incidence, the measured reflection and transmission coefficient of the proposed bandpass FSS is shown in Fig. 19(b) and 20(b) in different θ angles from 0° to 60°. It is observed that S-parameter magnitude is also stable for y-polarised and different angles similar to the x-polarised. Thus, the measured

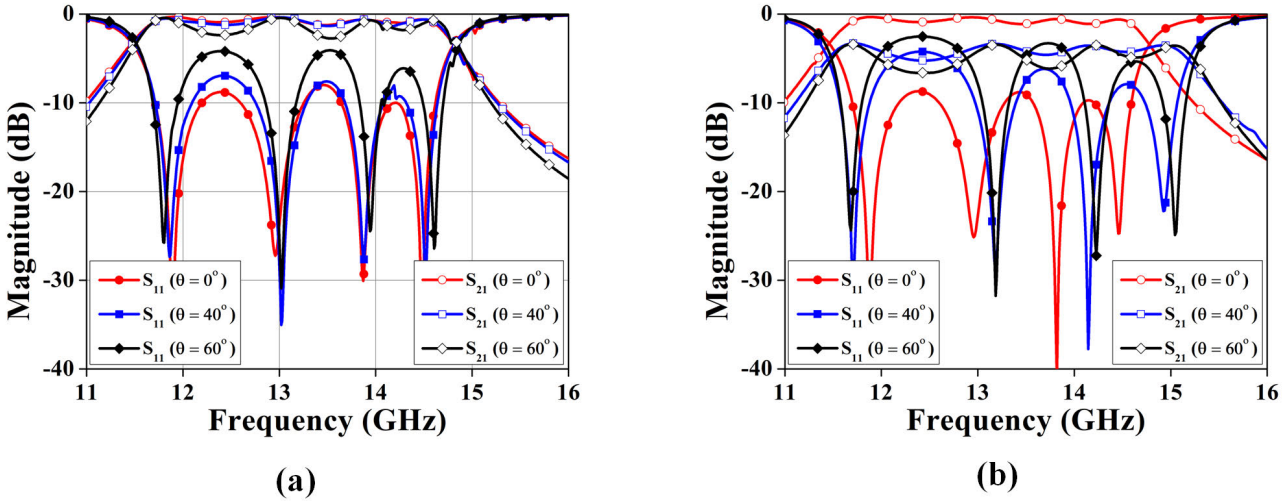

FIGURE 19. Reflection Loss $S11$ in dB and Phase in Deg, (a) x-polarized, (B) y-polarized (Physical parameters: a=8mm, b=5.3mm, b_1=1.3mm, h=0.813mm, ε_r = 3.55).

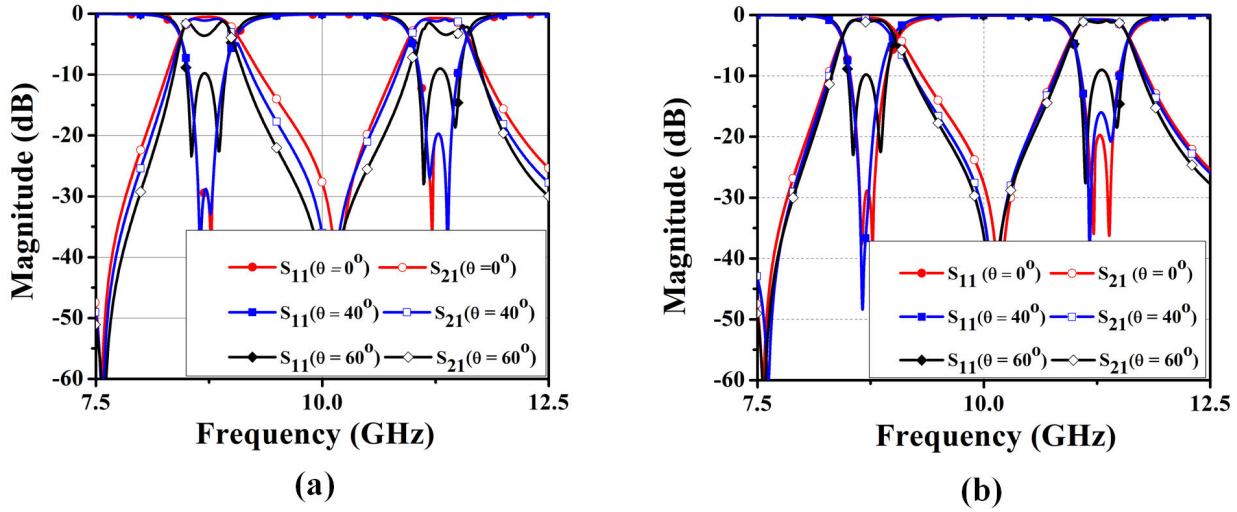

FIGURE 20. Reflection Loss $S11$ in dB and Phase in Deg, (a) x-polarized, (B) y-polarized (Physical parameters: a=8mm, b=6.7mm, b_1=1.3mm, h=0.406mm, ε_r = 3.55).

TABLE 1. Comparison between the proposed single band fourth order bandpass FSS and other designs.

Ref	Element strucuture	Number of mettalic layer	-3dB FBW	Element size (λ)	Polarization	Band ratio
13	3D structurebased on slot lines	-	75%	0.21	single	2
14	multilayer antenna filter antenna	5	36%	0.25	dual	1.48
17	antenna-filter-antenna	3	10%	0.63	single	1.37
18	aperture coupled fractal antenna	3	8.2%	0.471	single	-
22	cascaded SIW cavity	4	1.67%	0.72	dual	1.34
28	cascading slotline	2	62.75%	0.625	dual	2.66
In this work	aperture coupled single band patch resonator	3	21%	0.34	dual	1.18

TABLE 2. Comparison between the proposed dual band second order bandpass FSS and other designs.

Ref.	Element structure	No. of poles	Number of TZs	-3dB FBW	Band ratio	element size (λ)
6	Connected metallicplates and parallel-plate capacitors	1	1	26% / 33%	2	0.11
20	Composite aperture coupled patches	2	0	9% / 6%	1.37	0.6
23	Multilayer non-resonant structures	2	1	22% / 8%	1.35	0.17
27	Dielectric resonators with capped angular ring	2	2	17.5% / 14.5%	1.48	0.55
28	cascading slotline	4	0	62.75%	2.66	0.625
In this work	Aperture coupled dual mode second order patch resonators	2	2	6.1%/ 4.2%	1.25	0.34

minimum and maximum insertion loss (S_{21}) for the proposed FSS in range of is 0.2dB to 7.1dB for single band and for dual band ranges of is 0.1dB to 0.3dB, respectively.

The measured results show more insertion loss for single band relative to substrate roughness and fabricated FSS thickness. The proposed single band fourth order and dual band second order structure has a multilayer topology. As a result of the truncated edge patches and optimized apertures, the proposed structure has a band ratio of 1.18 and 1.25. However, the design features higher order and sharpening roll off traditional (AC-PRs). The work carried out and compared with different authors exhibits attractive advantages listed in Table 1 and Table 2. Comparing the simulated and measured results to those of various authors, the proposed design almost met expectations.

VI. CONCLUSION

In this article, a periodic higher order bandpass FSS has been proposed and demonstrated for single and dual band higher order filtering response. The operation principle of L-shape truncated square patch resonator has been analyzed to excite two orthogonal modes. Then, a combination of such four resonators rotated 90° between two adjacent patches to eliminate cross-polarized reflection caused by two orthogonal modes. next, a bandpass dual band FSS formed by two of such resonators are placed back-to-back manner through the coupling aperture presented as a middle metallic layer. Further, with the help of an equivalent circuit model, the principle of operation is examined. Finally, higher order bandpass FSS have been simulated, fabricated, and tested in a vector network analyzer (VNA). The measured results are good in agreement with simulated results, shows stable polarizations at different incident angles and polarizations. The proposed dual band second order bandpass FSS is good angular stability in conformal higher order Frequency selective surfaces.

REFERENCES

[1] B. A. Munk, *Frequency Selective Surfaces: Theory and Design*. New York, NY, USA: Wiley, 2000.

[2] T. K. Wu, *Frequency Selective Surface and Grid Array*. New York, NY, USA: Wiley, 1995.

[3] M. A. Al-Joumayly and N. Behdad, "Wideband planar microwave lenses using sub-wavelength spatial phase shifters," *IEEE Trans. Antennas Propag.*, vol. 59, no. 12, pp. 4542–4552, Dec. 2011.

[4] A. H. Abdelrahman, A. Z. Elsherbeni, and F. Yang, "Transmitarray antenna design using cross-slot elements with no dielectric substrate," *IEEE Antennas Wireless Propag. Lett.*, vol. 13, pp. 177–180, 2014.

[5] A. Aziz, F. Yang, S. Xu, and M. Li, "An efficient dual-band orthogonally polarized transmitarray design using three-dipole elements," *IEEE Antennas Wireless Propag. Lett.*, vol. 17, no. 2, pp. 319–322, Feb. 2018.

[6] P.-C. Zhao, Z.-Y. Zong, W. Wu, B. Li, and D.-G. Fang, "An FSS structure based on parallel LC resonators for multiband applications," *IEEE Trans. Antennas Propag.*, vol. 65, no. 10, pp. 5257–5266, Oct. 2017.

[7] A. K. Rashid, B. Li, and Z. Shen, "An overview of three-dimensional frequency-selective structures," *IEEE Antennas Propag. Mag.*, vol. 56, no. 3, pp. 43–67, Jun. 2014.

[8] K. Sarabandi and N. Behdad, "A frequency selective surface with miniaturized elements," *IEEE Trans. Antennas Propag.*, vol. 55, no. 5, pp. 1239–1245, May 2007.

[9] R. Phon, S. Ghosh, and S. Lim, "Active frequency selective surface to switch between absorption and transmission band with additional frequency tuning capability," *IEEE Trans. Antennas Propag.*, vol. 67, no. 9, pp. 6059–6067, Sep. 2019.

[10] F. Bayatpur and K. Sarabandi, "Multipole spatial filters using metamaterial-based miniaturized-element frequency-selective surfaces," *IEEE Trans. Microw. Theory Techn.*, vol. 56, no. 12, pp. 2742–2747, Dec. 2008.

[11] B. Li and Z. Shen, "Bandpass frequency selective structure with wideband spurious rejection," *IEEE Antennas Wireless Propag. Lett.*, vol. 13, pp. 145–148, 2014.

[12] B. Li and Z. Shen, "Dual-band bandpass frequency-selective structures with arbitrary band ratios," *IEEE Trans. Antennas Propag.*, vol. 62, no. 11, pp. 5504–5512, Nov. 2014.

[13] B. Li, L. Zhu, Y. Tang, Y. Chang, Y. Han, and Y. Lyu, "Wideband frequency selective structures based on stacked microstrip/slot lines," in *Proc. Int. Conf. Microw. Millim. Wave Technol. (ICMMT)*, Chengdu, China, May 2018, pp. 1–3.

[14] Y. Li, L. Li, Y. Zhang, and C. Zhao, "Design and synthesis of multilayer frequency selective surface based on antenna-filter-antenna using Minkowski fractal structures," *IEEE Trans. Antennas Propag.*, vol. 63, no. 1, pp. 133–141, Jan. 2015.

[15] R. Pous and D. M. Pozar, "A frequency-selective surface using aperture-coupled microstrip patches," *IEEE Trans. Antennas Propag.*, vol. 39, no. 12, pp. 1763–1769, Dec. 1991.

[16] D. S. Wang, P. Zhao, and C. H. Chan, "Design and analysis of a high-selectivity frequency-selective surface at 60 GHz," *IEEE Trans. Microw. Theory Techn.*, vol. 64, no. 6, pp. 1694–1703, Jun. 2016.

[17] A. Abbaspour-Tamijani, K. Sarabandi, and G. M. Rebeiz, "Antenna-filter-antenna arrays as a class of bandpass frequency-selective surfaces," *IEEE Trans. Microw. Theory Tech.*, vol. 52, no. 8, pp. 1781–1789, Aug. 2004.
[18] J. A. Curtis and S. J. Fiedziuszko, "Multi-layered planar filters based on aperture coupled, dual mode microstrip or stripline resonators," in *IEEE MTT-S Int. Microw. Symp. Dig.*, Jun. 1992, pp. 1203–1206.
[19] Q. Zhou, P. Liu, K. Wang, H. Liu, and D. Yu, "Absorptive frequency selective surface with switchable passband," *Int. J. Electron. Commun.*, vol. 89, pp. 160–166, May 2018.
[20] H. Zhou, S. Qu, B. Lin, J. Zhang, C. Gu, H. Ma, Z. Xu, P. Bai, and W. Peng, "Dual band frequency selective surface based on circular aperture-coupled patches," *Microw. Opt. Technol. Lett.*, vol. 53, no. 8, pp. 1784–1786, Aug. 2011.
[21] C. A. Balanis, *Antenna Theory: Analysis and Design*. New York, NY, USA: Wiley, 1997.
[22] G. Q. Luo, W. Hong, H. J. Tang, and K. Wu, "High performance frequency selective surface using cascading substrate integrated waveguide cavities," *IEEE Microw. Wireless Compon. Lett.*, vol. 16, no. 12, pp. 648–650, Dec. 2006.
[23] M. Al-Joumayly and N. Behdad, "A new technique for design of low-profile, second-order, bandpass frequency selective surfaces," *IEEE Trans. Antennas Propag.*, vol. 57, no. 2, pp. 452–459, Feb. 2009.
[24] B. Li, X. Huang, L. Zhu, Y. Zhang, Y. Tang, W.-J. Lu, and Y. Bo, "Bandpass frequency selective structure with improved out-of-band rejection using stacked single-layer slotlines," *IEEE Trans. Antennas Propag.*, vol. 66, no. 11, pp. 6003–6014, Nov. 2018.
[25] Z. Zhang, X. Li, C. Sun, Y. Liu, and G. Han, "Dual-band focused transmitarray antenna for microwave measurements," *IEEE Access*, vol. 8, pp. 100337–100345, 2020.
[26] S. Qiu, Q. Guo, and Z. Li, "Tunable frequency selective surface based on a sliding 3D-printed inserted dielectric," *IEEE Access*, vol. 9, pp. 19743–19748, 2021.
[27] B. Zhang, C. Jin, X. Ye, and R. Mittra, "Dual-band dual-polarized quasi-elliptic frequency selective surfaces," *IEEE Antennas Wireless Propag. Lett.*, vol. 18, pp. 298–302, 2019.
[28] H. Li, B. Li, and L. Zhu, "Direct synthesis and design of wide-band linear-to-circular polarizers on 3-D frequency selective structures," *IEEE Trans. Antennas Propag.*, vol. 70, no. 10, pp. 9385–9395, Oct. 2022.

K. N. MOHAN (Student Member, IEEE) received the M.S. degree in antenna and wave propagation from Vellore Institute of Technology, Vellore, India, in 2017, where he is currently pursuing the Ph.D. degree in antennas and wireless communication. He has been an Assistant Professor with the Koneru Lakshmaiah Educational Foundation (KLEF), Vijayawada. He has published research papers in several journals and conferences. His research interests include frequency selective surfaces, phased array antennas, and UWB microstrip antennas. He is a Reviewer of the research article for *Turkish Journal of Electrical Engineering and Computer Sciences*.

YOGESH KUMAR CHOUKIKER (Senior Member, IEEE) received the B.E. degree, in 2007, and the M.Tech. and Ph.D. degrees in electronics engineering from the National Institute of Technology, Rourkela, Orissa, India, in 2009 and 2014, respectively. He specialized in antenna and wave propagation. He was a Visiting Research Scholar with San Diego State University, San Diego, CA, USA, during the Ph.D. studies. Since January 2014, he has been a Professor with Vellore Institute of Technology, Vellore. He completed the ISRO respond project, in 2013, which is based on optimization techniques. He has completed two SERB Government of India projects. He has published more than 70 research papers in referred journals and international conferences/symposia. His research interests include microstrip antenna (fractal antennas) in the area of wireless applications, MIMO environment, UWB, and reconfigurable fractal. He is a Reviewer of the research article of IEEE TRANSACTIONS ON ANTENNAS AND PROPAGATION, IEEE TRANSACTIONS ON MICROWAVE AND THEORY TECHNIQUES, IEEE ANTENNAS AND WIRELESS PROPAGATION LETTERS, *International Journal of RF and Microwave Computer-Aided Engineering*, and *IET Microwave, Antennas, and Propagation*.